

The Advanced LIGO Gravitational Wave Detector

S. J. Waldman, for the LIGO Scientific Collaboration

LIGO Laboratory, Kavli Institute for Astrophysics and Space Research, MIT NW22-270, 185 Albany St., Cambridge MA 02139

The Advanced LIGO gravitational wave detectors will be installed starting in 2011, with completion scheduled for 2015. The new detectors will improve the strain sensitivity of current instruments by a factor of ten, with a thousandfold increase in the observable volume of space. Here we describe the design and limiting noise sources of these second generation, long-baseline, laser interferometers.

1 Introduction

Einstein's general theory of relativity predicts the existence of gravitational waves (GWs), oscillations in the space-time metric that propagate at the speed of light. The Laser Interferometer Gravitational-Wave Observatory, LIGO, is designed to detect and study astrophysical GWs, with the promise of studying qualitatively new physics and astrophysics. [1] In particular, the direct detection of GWs will provide information about systems in which strong-field gravitation dominates, a virtually untested regime in which space-time curvature self-interacts. Such GW sources include compact binary coalescences in which a neutron star or black hole binary system inspirals together, coalescing to form a black hole; the stellar core collapse thought to power Type II supernovae; rapidly rotating asymmetric neutron stars; and possibly cosmic-scale processes that produce a stochastic background of GWs. [2]

In the past few years, the first generation of long-baseline gravitational wave detectors has successfully operated at or near design sensitivity. In collaboration with the Virgo 3 km and the GEO 600 m interferometers, [3, 4] LIGO anchors a worldwide network of instruments in search of the first direct detection of gravitational waves. The LIGO detectors operated from November 2005 to October 2007, with joint data taking with Virgo starting in May 2007. The data is currently being analyzed for GW signals from inspiraling binary systems, burst sources, a stochastic GW background, and rapidly rotating neutron stars. The status of these searches and their astrophysical importance is discussed by other authors in these proceedings.

This article focuses on the next generation of LIGO interferometers, in particular Advanced LIGO, currently being designed and assembled at two sites in the United States. The Livingston Parish, Louisiana observatory will operate a single interferometer, L1, with 4 km long arms while the Hanford, Washington observatory will operate two 4 km interferometers within a common vacuum envelope, H1 and H2. The second generation Advanced LIGO detectors will improve the sensitivity of ground-based gravitational wave detectors by an order of magnitude over current detectors. A preliminary Advanced LIGO design was described in Ref. [5], here we provide an overview of the final design as construction begins. We first describe the Advanced LIGO optical configuration, then follow with a description of the dominant noise terms and anticipated

sensitivities. Finally, we conclude with comments on the initial tests of Advanced LIGO and progress towards the first science runs.

2 Advanced LIGO Optical Design

From a detector perspective, gravitational waves can be thought of as a quadrupole strain of space, $h = \delta L/L$, which can be probed by monitoring the relative positions of inertial test masses with light. Equivalently, in a fixed Lorentzian frame, gravitational waves create a tidal force, a force proportional to the distance from a chosen origin. As with electromagnetic waves, GWs are transverse waves that travel at the speed of light. Unlike electromagnetism, GWs are constrained by mass and momentum conservation to be quadrupolar: the strain (or tidal forces) contracts along one transverse dimension while expanding the orthogonal dimension. Also unlike electromagnetism, GWs are very weak and interact very weakly as they propagate through space; detectable GWs are generated only by the coherent acceleration of stellar masses at relativistic velocities. The strongest nearby sources will produce strains on Earth no larger than $h \approx 10^{-21}$. Finally, it's worth noting that GW detectors measure the amplitude of a GW (as opposed to the power) so that the observed volume of space scales cubically with the detector sensitivity.

The Advanced LIGO optical design consists of a Michelson interferometer with Fabry-Perot arm cavities, a power recycling cavity and a signal recycling cavity as shown in Fig. 1. The Michelson topology is well matched to the quadrupole strain: a properly oriented, linearly polarized GW propagating normal to the interferometer plane generates a positive strain along one arm, a negative strain along the other and vice versa, oscillating in time. In the Advanced LIGO configuration, the arm lengths are controlled so that Michelson interferometer reflects the input laser beam back towards the laser while the anti-symmetric port is dark. The differential motions of the two arms – the GW signal – constructively interfere at the beam splitter's Anti-Symmetric port, labeled "AS" in Fig. 1. The common mode signals generated by common mode motion of the end mirrors, by laser frequency noise, and by laser intensity noise constructively interfere at the beam splitter's Symmetric port; to first order, this configuration eliminates laser technical noise couplings to the GW signals.

Fabry-Perot cavities in the interferometer arms defined by the partially reflecting Input Test Mass (ITM) and high reflectance End Test Mass (ETM) resonate the input laser light to increase the power in the arms. Similarly, the partially reflecting Power Recycling Mirror (PRM) resonates the light that returns toward the laser from the beam splitter's symmetric port. Together the arm and power recycling cavities build up the laser power in the arms by a factor of $\simeq 6000$. The power recycled Fabry-Perot Michelson topology is identical to Initial LIGO and has been described in detail in Ref. [6].

Advanced LIGO has several significant changes in the optics relative to Initial LIGO: the Signal Recycling Mirror (SRM) is added to the AS port of the interferometer to form a signal recycling cavity, the power and signal recycling cavities have a stable geometry, the GW signal is detected using DC readout, and the laser power is increased. The SRM forms a resonant cavity for the differential mode signal, altering the interferometer dynamics. [7, 8] The impact on the interferometer quantum noise is discussed further in the §3.3 below.

In Initial LIGO, the ≈ 10 m long power recycling cavity was formed by mirrors having ≥ 10 km radii of curvature, effectively a flat-flat resonator geometry. That configuration was extremely sensitive to changes in the curvatures caused by unavoidable thermal lensing. To reduce the thermal sensitivity, the Advanced LIGO signal and power recycling cavities are each formed by a folded chain of three curved mirrors. In effect, the Advanced LIGO recycling cavities incorporate beam expanding telescopes that reduce the sensitivity to thermal lenses in the ITMs. In a similar change, the Fabry-Perot arm cavities have a near concentric configuration

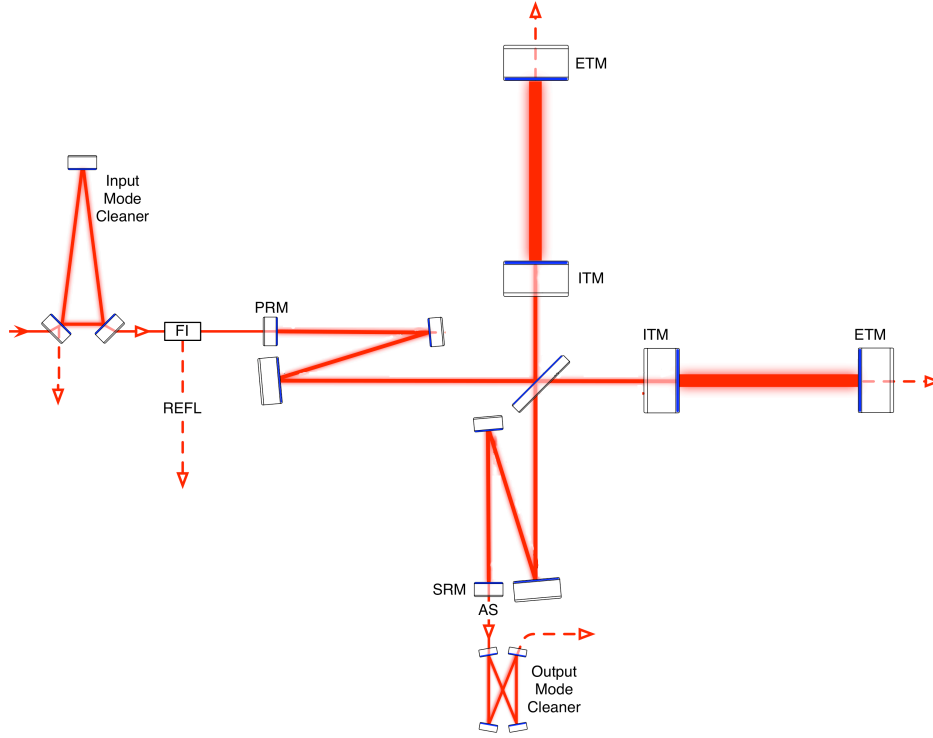


Figure 1: The Advanced LIGO optical layout. The triangular suspended input mode cleaner filters frequency and amplitude noise from the laser (not shown) and provides a stable input beam. The Faraday Isolator (FI) isolates the laser from the interferometer reflected beam (REFL) used to control the laser frequency. The 4 km long Fabry-Perot arm cavities are formed between the ITM and ETM test masses. The Power Recycling Mirror (PRM) and Signal Recycling Mirrors (SRM) form folded cavities discussed in the text. The GW signals are carried by the light transmitted through the Output Mode Cleaner at the Anti-Symmetric (AS) port.

motivated by the reduced coating thermal noise from large spot sizes, discussed in §3.2, and from the improved response to optical torques for near concentric cavities, discussed in Ref. [9].

The Advanced LIGO differential arm length will be detected in a homodyne scheme known as DC readout. In DC readout, the GW signals are measured directly as amplitude modulations on a static field at the AS port. The static field is created by a small offset in the differential arm length; GWs make oscillations around the offset, modulating the output. However, many fields are present at the AS port that don't carry GW information such as auxiliary control fields and scattered non-resonant light. Advanced LIGO incorporates an Output Mode Cleaner (OMC) at the AS port to select only those fields containing GW signal. The OMC is a ~ 1 m long optical cavity which filters the interferometer output before detection, transmitting only light from the arm cavity.

Finally, the Initial LIGO laser will be upgraded from a 10 W Master Oscillator/Power Amplifier (MOPA) to a 180 W MOPA for Advanced LIGO. [10] The input optics are upgraded to match the laser: high power versions of electro-optic phase modulators, photodetectors, and Faraday isolators replace conventional components. With these changes, the maximum Advanced LIGO arm power approaches 800 kW, improving the shot noise limited sensitivity by a factor of ≈ 6 with respect to Initial LIGO.

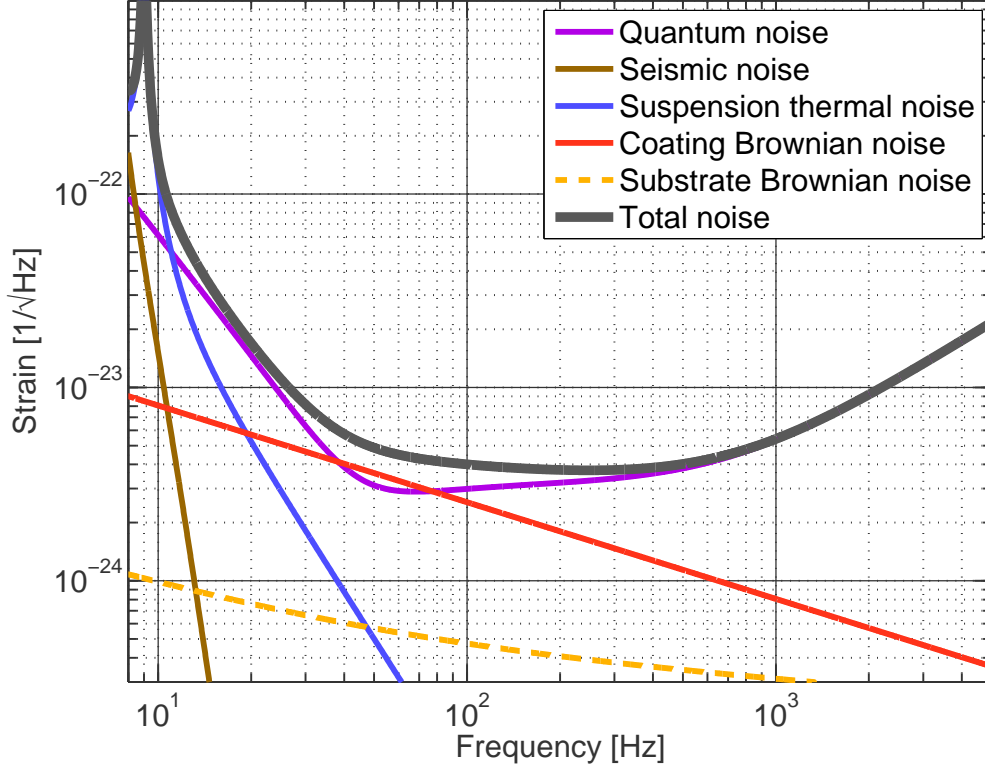


Figure 2: The modeled noise budget for an Advanced LIGO interferometer with $\phi_{SRM} = 0$ and 125 W input power. The total noise (grey) is the incoherent sum of each of the listed noise terms, described in detail below.

3 Advanced LIGO Noise Contributions

The Advanced LIGO sensitivity limits are estimated from calculations of technical and fundamental noises; many of these have been studied with Initial LIGO and other dedicated experiments.^a Below 10 Hz, the sensitivity is limited by the seismic motion of the earth, at intermediate frequencies thermal noise dominates, and at the highest frequencies photon shot noise limits the sensitivity. The interferometer noise contributions, modeled with the GWINC-v2 software package and plotted in Fig. 2, are described in the following sections.

3.1 Acoustic and Seismic Isolation

The Advanced LIGO detector requires a residual RMS differential arm motion of $\delta x \leq 10^{-15}$ m to maintain the arm power buildup and to minimize the coupling of laser noise into the GW signal. In the GW detection band, the required test mass displacement is $\delta x \leq 10^{-19} m/\sqrt{Hz}$ at 10 Hz and $\delta x \leq 2 \times 10^{-20} m/\sqrt{Hz}$ at 100 Hz. Here, δx refers only to the differential arm motion; the common arm motion and the motion of the other length degrees of freedom may be somewhat larger. To meet these requirements, the interferometer is isolated from environmental influences such as acoustic noise, gas produced phase noise, and seismic noise. Thus, the interferometer optics are enclosed in an ultra-high vacuum system. The facility specifications have been determined by the standard quantum sensitivity limit for a future interferometer with 1 ton test masses. The $\simeq 10^{-9}$ torr vacuum reduces the gas produced phase noise to an equivalent strain of $h \approx 10^{-25}$, well below the anticipated Advanced LIGO sensitivity. In addition, the interferometer detection beam paths, including the photodetectors, are enclosed within the vacuum on the seismic isolation platforms to eliminate acoustic coupling and reduce

^aSee Ref. [6] and references therein.

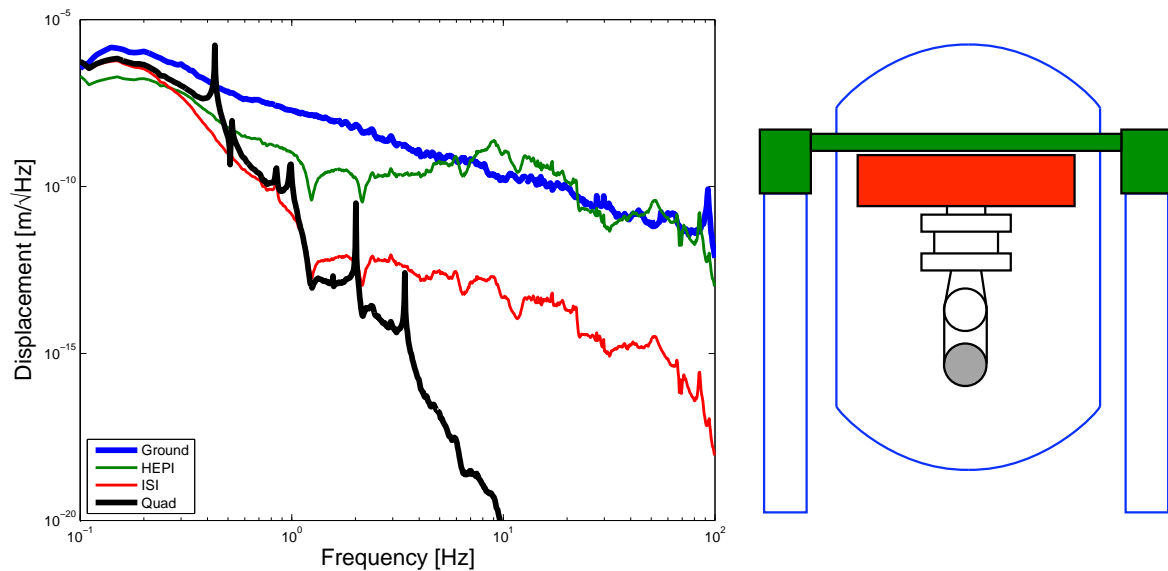


Figure 3: The Advanced LIGO seismic isolation consists of several stacked stages of active isolation shown schematically on the right, with colors matching the curve and the test mass shaded gray. The reference ground motion (blue) is the average ground displacement at the Livingston observatory. The HEPI curve (green) is the motion atop the hydraulic pre-isolator located outside the vacuum system. The anticipated ISI payload motion (red) is calculated from models of the two stage active isolator performance with the HEPI motion as the input spectrum. The motion of the test mass at the end of the four-stage suspension is calculated from a model and shown in the Quad curve (black).

the motion of light scatterers.

Isolating the interferometer optics from ground motion is a task divided into several stages, with each stage providing isolation for the following stage. The effect of each stage of isolation can be seen in Fig. 3. At the lowest frequencies, an active, 6 degree of freedom, hydraulic, external pre-isolator (HEPI) reduces the motion between 0.1 and 5 Hz by a factor of $\simeq 10$. [11] A two stage, active, internal seismic isolation (ISI) system enclosed within the vacuum reduces ground motion by a further factor of $\simeq 300$ at 1 Hz and $\simeq 3000$ at 10 Hz. [12] Both active isolation systems consist of a spring mounted, actuated platform outfitted with a suite of motion sensors. The sensors measure the platform motion and feedback to the actuators, thereby stabilizing the platform to a level limited by the sensor noise floors and mechanical cross coupling.

The interferometer optics are suspended from the ISI platforms using a coupled pendulum system based on the GEO-600 three-stage suspensions. [13] The beam splitter, power recycling cavity and signal recycling cavity optics are hung from three-stage suspensions consisting of two metal masses linked with steel wire, followed by the optic itself. Vertical isolation is provided by cantilevered blade springs mounted to the metal masses. Above the pendulum resonances, the triple suspension provides isolation proportional to $1/f^6$. The ITMs and ETMs are suspended from four-stages consisting of two metal masses with vertical springs, a fused silica intermediate mass, and the test mass. Welded fused silica fibers join the test mass to the fused silica mass above. [14] The additional isolation stage is necessary to meet the displacement noise goals at 10 Hz, and the fused silica fibers reduce the thermal noise as discussed below. Altogether, the Advanced LIGO isolation systems reduce the seismic-induced test mass motion by 10 orders of magnitude to $\delta x \simeq 10^{-20} m/\sqrt{Hz}$ at 10 Hz, opening the frequency band from 10 to 40 Hz for gravitational wave searches.

3.2 Thermal Noise Sources

Between 10 and 200 Hz, thermal noise sources limit the interferometer sensitivity. An unavoidable consequence of energy dissipation, thermal noise is modeled by applying the fluctuation-dissipation theorem to all aspects of the system which influence the motion or measurement of the arm cavity test masses. The fluctuation dissipation theorem is closely related to Brownian motion, hence thermal noise associated with mechanical motion is often called Brownian noise. Three sources of dissipation dominate the Advanced LIGO thermal noise: mechanical loss in each test mass leads to fluctuations in the mirrored surface of the test mass; dissipation within the suspension fibers generates a fluctuating force on the test masses; and losses within the mirror's dielectric coating generate a fluctuating phase shift of the reflected light.

The test mass mechanical loss determines the level of substrate Brownian noise that causes fluctuations of the surface with respect to the center of mass. Early Advanced LIGO designs considered sapphire test masses for their superior mechanical and thermal properties. [15] Since then, fused silica test masses have demonstrated sufficiently low loss and have been adopted as the substrate material. The Advanced LIGO test masses are 40 kg, high purity, low-inclusion fused silica cylinders 34 cm in diameter. To maintain the substrates' excellent mechanical properties, no lossy materials contact the test mass (eg. magnets). The masses are suspended via fused silica mounting blocks hydroxy-catalysis bonded to each side. [16] Fused silica fibers are welded to the blocks and connect to the upper fused silica mass in a similar fashion. The test masses are actuated using a non-contact, low-force and low-noise electrostatic drive. As a result of these measures, the test masses have very low loss (mechanical quality factors exceeding 10^7), and correspondingly low fluctuations, contributing to the strain noise at $h \approx 3 \times 10^{-24} f^{-1/2} \text{ Hz}^{-1/2}$.

Loss in the mechanical structure supporting the test masses generates fluctuating forces at the masses' suspension points. [17] The extremely low mechanical loss needed to limit the fluctuations motivates the fused silica fiber stage of the four-stage suspension. Since the loss is dominated by the bending regions near the fiber ends, the cylindrical fibers are laser polished and drawn from fused silica rod with a carefully controlled, variable diameter. At the ends where the fiber is welded to the test mass, the fibers have a large diameter to reduce flexing of the (potentially higher loss) welded joints. The fibers then taper with an optimized profile so that the bending occurs predominantly in a low loss region of the fiber. Suspension thermal noise contributes to the detector noise below 30 Hz, limiting the low-frequency sensitivity to $h \approx 2 \times 10^{-21} f^{-2} \text{ Hz}^{-1/2}$.

Finally, thermal noise from the dielectric mirror coatings limits the detector noise between 40 and 140 Hz, the most sensitive region. The coatings are alternating layers of SiO_2 and titanium-doped TaO_2 . [18] Both thermo-optic and mechanical loss contribute to the thermal noise. The thermo-optic noises include thermo-refractive fluctuations in the layers' index of refraction as well as the thermo-elastic fluctuations that modify the layer thickness and hence the magnitude and phase of the reflected field. The coating mechanical loss dominates the thermal noise by an order of magnitude, primarily in the thick ETM high reflector. Because the thin film coatings have a high mechanical loss relative to the substrate, the coating Brownian noise exceeds that of the substrate by nearly an order of magnitude. The coating noise is inversely proportional to the beam diameter, motivating large spot sizes on the optics as described in §2. Coating thermal noise limits the detector sensitivity to $h \approx 2.5 \times 10^{-23} f^{-1/2} \text{ Hz}^{-1/2}$.

3.3 Quantum Noise

Quantum mechanics limits the precision at which the test mass positions can be determined. At high frequencies, photon shot noise limits the sensitivity to $h \propto \sqrt{f/P}$, while at low frequencies radiation pressure limits the sensitivity to $h \propto \sqrt{P}/f^2$. The Advanced LIGO interferometer is a realization of a Heisenberg microscope: the high laser power required to determine the position of

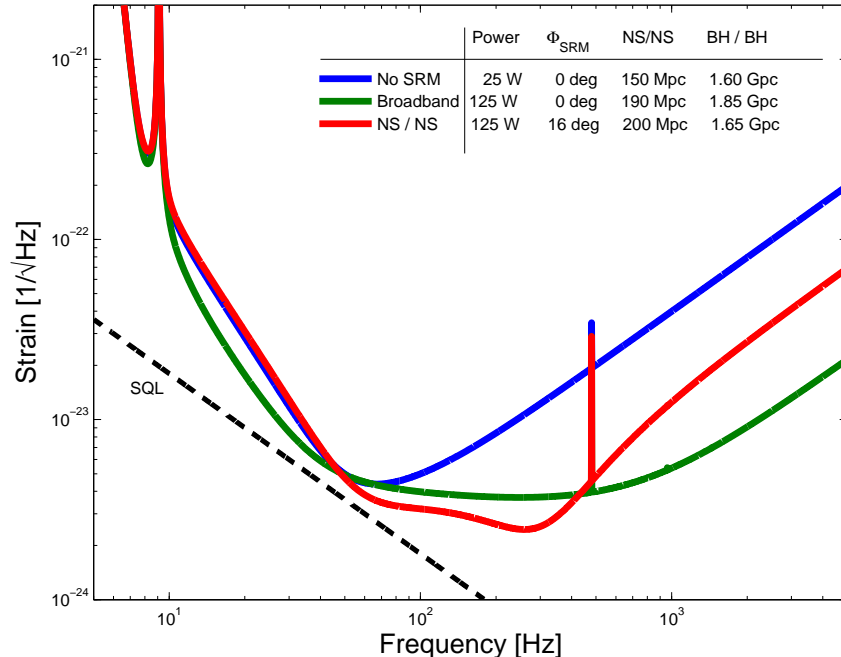


Figure 4: Amplitude spectral densities of the anticipated sensitivities of the Advanced LIGO interferometers as a function of the tuning of the signal recycling phase, ϕ_{SRM} . **No SRM** is a potential initial interferometer configuration with no signal recycling mirror with modest sensitivity; the **Broadband** configuration has good sensitivity at all frequencies; and **NS/NS** is optimized for the detection of two coalescing $1.4 M_{\odot}$ neutron stars.

the test masses exerts a fluctuating radiation pressure which perturbs the test mass positions. In the absence of position-momentum correlations, the Advanced LIGO strain sensitivity is limited by the Standard Quantum Limit (SQL) $h_{SQL} = 1.8 \times 10^{-22}/f \text{ Hz}^{-1/2}$. Because the signal recycling cavity couples the test mass position and momentum, sub-SQL sensitivity is possible over a frequency bandwidth $\Delta f \sim f$ at the expense of the sensitivity at other wavelengths. [19] The primary difference between the three curves shown in Fig. 4 is the degree of correlation between the test mass position and momentum as determined by the SRM reflectivity and the signal recycling cavity length tuning.^b The noise curves include the thermal and seismic noises calculated by GWINC-v2.

4 Advanced LIGO Progress

Some Advanced LIGO hardware has already been installed on the Initial LIGO interferometers. These components include: a 35 W laser Master-Oscillator/Power-Amplifier; a high-power, in vacuum Faraday Isolator; a single stage, in-vacuum seismic isolation system; and DC readout using an in-vacuum Output Mode Cleaner. With these systems, LIGO has begun another science run, the sixth, with significantly improved high frequency performance.

The Advanced LIGO project began in 2008, with plans for the first in-vacuum hardware installation in early 2011. To evaluate the greatly increased chances for direct GW detection, we consider compact binary coalescences for which the source rate can be estimated from observed binary pulsar systems. Once the instruments reach the anticipated sensitivities, we can expect to detect between 1 and 1,000 compact binary coalescences per year. As installation and commissioning progress, Advanced LIGO will transform the field from searching for the first direct GW detection to exploring the rich phenomena of GW astrophysics.

^bThese noise curves can be found at <https://dcc.ligo.org/cgi-bin/private/DocDB/ShowDocument?docid=2974> and the documents therein.

Acknowledgments

We gratefully acknowledge the support of the United States National Science Foundation for the construction and operation of the LIGO Laboratory and the Science and Technology Facilities Council of the United Kingdom, the Max-Planck-Society, and the State of Niedersachsen/ Germany for support of the construction and operation of the GEO600 detector. We also gratefully acknowledge the support of the research by these agencies and by the Australian Research Council, the Council of Scientific and Industrial Research of India, the Istituto Nazionale di Fisica Nucleare of Italy, the Spanish Ministerio de Educacion y Ciencia, the Conselleria d'Economia Hisenda i Innovacio of the Govern de les Illes Balears, the Scottish Funding Council, the Scottish Universities Physics Alliance, The National Aeronautics and Space Administration, the Carnegie Trust, the Leverhulme Trust, the David and Lucile Packard Foundation, the Research Corporation and the Alfred P Sloan Foundation.

References

- [1] A Abramovici. LIGO: The Laser Interferometer Gravitational-Wave Observatory. *Science*, 256:325–333, 1992.
- [2] Curt Cutler and Kip S Thorne. An Overview of Gravitational-Wave Sources. *eprint arXiv*, page 4090, 2002.
- [3] F Acernese, M Alshourbagy, et al. Virgo status. *Class. Quantum Grav*, 25:4001, 2008.
- [4] B Willke. The GEO 600 gravitational wave detector. *Class. Quantum Grav*, 19:11, 2002.
- [5] P Fritschel. Second generation instruments for the Laser Interferometer Gravitational Wave Observatory (LIGO). *Proceedings of SPIE*, 4856, 2003.
- [6] B. P Abbott et al. LIGO: the Laser Interferometer Gravitational-Wave Observatory. *Reports on Progress in Physics*, 72:6901, 2009.
- [7] B Meers. Recycling in laser-interferometric gravitational-wave detectors. *PhysRev D*, 1988.
- [8] J Mizuno, K. A Strain, P. G Nelson, et al. Resonant sideband extraction: a new configuration for interferometric gravitational wave detectors. *Physics Letters A*, 175:273, 1993.
- [9] J Sidles and D Sigg. Optical torques in suspended Fabry–Perot interferometers. *Physics Letters A*, 354(3):167–172, 2006.
- [10] B Willke, K Danzmann, M Frede, et al. Stabilized lasers for advanced gravitational wave detectors. *Class. Quantum Grav*, 25:4040, 2008.
- [11] Fritschel, A Ganguli, J Giaime, et al. Seismic isolation enhancements for initial and advanced LIGO. *Class. Quantum Grav*, 2004.
- [12] R. Abbott et al. Seismic isolation for Adv. LIGO. *Class. Quantum Grav*, 19:1591, 2002.
- [13] M. V Plissi, C. I Torrie, M. E Husman, et al. GEO 600 triple pendulum suspension system: Seismic isolation and control. *Review of Scientific Instruments*, 71:2539, 2000.
- [14] N. A Robertson, G Cagnoli, D. R. M Crooks, et al. Quadruple suspension design for Advanced LIGO. *Class. Quantum Grav*, 19:4043, 2002.
- [15] S Rowan, G Cagnoli, P Sneddon, et al. Investigation of mechanical loss of candidate materials for the test masses of gravitational wave detectors. *Phys. Letters A*, 265:5, 2000.
- [16] S Rowan, S. M Twyford, J Hough, et al. Mechanical losses associated with the technique of hydroxide-catalysis bonding of fused silica. *Physics Letters A*, 246:471, 1998.
- [17] G Gonzalez. Suspensions thermal noise in the LIGO gravitational wave detector. *Class. Quantum Grav*, 2000.
- [18] Gregory M Harry, Matthew R Abernathy, Andres E Becerra-Toledo, et al. Titania-doped tantala/silica coatings for gravitational-wave detection. *Class. Quantum Grav*, 24:405, 2007.
- [19] A Buonanno and Y Chen. Quantum noise in second generation, signal-recycled laser interferometric gravitational-wave detectors. *Physical Review D*, 64:042006, 2001.